Unsupervised Dynamic Graph Multi-Model Representation Learning for Temporal Patterns Discovery: Uncovering Parkinson's Disease Stages Using Cerebrospinal Fluid Longitudinal Profiles

Anonymous authors

000

001

002

004

006

008

010

019

021

023

024

025

026

027

028

029

031

034

039

040

041

042

043

044

045

046

048

052

Paper under double-blind review

ABSTRACT

Existing dynamic graph learning methods typically encode node features at each time step by leveraging local (spatial/ structural) and/or short-range temporal dependencies. In contrast, we propose a novel multi-model framework that generates a representation for each node at every graph snapshot, where each representation encodes the node's temporal trajectory across the full sequence while preserving its spatial context within that specific time step. When clustered, these representations reveal meaningful temporal pattern groups in longitudinal datasets. This approach was evaluated in the context of Parkinson's disease (PD), a degenerative disorder that progresses in distinct clinical stages. To demonstrate this, we structured six years of longitudinal cerebrospinal fluid (CSF) records from 24 patients with PD into age-based graphs, where clinical visit records corresponding to patients with the same age are hosted on the graph for that age. In these graphs, nodes represent individual patients indexed by unique identifiers and are enriched with CSF peptide abundance features. Edges are established between patient nodes based on the similarity of their peptide expression patterns. For each patient's node, a one-layer Graph Convolutional Network (GCN) was employed to encode inter-patient relationships within each age-specific graph. The resulting spatial representations across all time points for each node were then fed into a sequential model to learn a unified spatial-temporal features representation for every patient. To represent patients' features at each age, the unified embedding was combined with the age-specific GCN representation through a fusion block - composed of linear transformations, nonlinear activations, and normalization layers - producing rich, locally informed spatial embeddings that are further enhanced by the global context of inter- and intra-related node patterns. K-means++ clustering of the multi-model representations identified four distinct disease stages, supported by strong cluster validity metrics (Davies-Bouldin Index = 0.169, Calinski-Harabasz Index = 1264.24). When statistically analyzed, the Kruskal-Wallis test revealed significant differences in motor scores (UPDRS_2 and UPDRS_3; p<0.05) across clusters, with Dunn's test further identifying which clusters differed significantly. Unlike the motor scores, which appeared to cluster most patient profiles into two groups, the non-motor scores (UPDRS_1) were distributed across three clusters but did not show significant differences (p = 0.11). The learned embeddings revealed well-separated clinical motor profiles, outperforming PCA, autoencoders, GCN, T-GCN, and GC-LSTM representations in capturing clinically relevant dimensions of disease severity. With further optimization and validation, this framework could aid in staging and understanding neurodegenerative diseases and generalizes to other longitudinal pattern discovery tasks.

1 Introduction

Graph Neural Networks (GNNs) have emerged as powerful tools for learning from graph-structured data by capturing nodes' local and global dependencies. Unlike traditional deep learning models, GNNs are not restricted to grid-like or strictly sequential input limits. This makes them well-suited for tasks involving complex and time-variant relationships among nodes features - dependencies that are often overlooked by conventional deep learning models such as Long Short-Term Memory (LSTM) networks and Convolutional Neural Networks (CNNs) de Jong et al. (2019); Çağatay Berke Erdaş et al. (2021); Gan et al. (2021); Li et al. (2021). For example, Dynamic Graph Neural Networks (DGNNs) have been developed to model every node's spatial and temporal variants in a sequence of graphs Wu et al. (2024); Zheng et al. (2024).

However, these generated embeddings often capture either local node relationships, such as embeddings learned by a Graph Convolutional Network (GCN), and/or short-term historical temporal patterns, like hidden state representations learned commonly by models like Temporal GCNs (T-GCN) and Graph Convolution Embedded LSTM networks (GC-LSTM). Although these approaches have shown effectiveness in supervised tasks such as node classification, feature prediction, and edge inference, they have been underexplored in unsupervised representation learning tasks, and fall short particularly when modeling long-range spatio-temporal dependencies is required Zheng et al. (2024). While existing graph learning models are capable of capturing feature relationships within individual nodes, across nodes, and over time, a key limitation remains: their inability to include generalized temporal dynamics alongside local structural patterns to create comprehensive embeddings for each node at every graph snapshot.

Bridging this gap is critical for advancing unsupervised representation learning in longitudinal data, particularly for uncovering temporal progression patterns in abnormally evolving processes or conditions. Motivated by the GCN's ability to capture local spatial patterns within a single graph snapshot and the strength of sequential models in capturing temporal dependencies, this study proposes a multi-model dynamic graph learning algorithm for modeling longitudinal records. Specifically, the model is designed to identify distinct temporal disease stages in the context of Parkinson's Disease (PD) progression case study. PD is the second most common progressive neurodegenerative disorder, with an estimated 11.77 million people worldwide in 2021 living with PD, and this number is projected to rise to 25.2 million by 2050 Luo et al. (2025); Su et al. (2025). PD abnormally evolves by time and manifests by motor symptoms and non-motor symptoms (such as mood changes), with an average survival of approximately nine years following symptom onset Ryu et al. (2023); Kouli et al. (2018). The exact cause and clinical trajectory of PD remain unclear and vary significantly between individuals due to the disease's inherent heterogeneity Balestrino & Schapira (2020); Abu Zohair et al. (2025).

Static graph models were increasingly applied to model data involving biomolecules, drugs, or patient-related features, such as clinical measurements or medication records Liu et al. (2025); Shang et al. (2019); Abu Zohair et al. (2025). While they have shown promise, they are inherently limited in capturing the temporal changes inherent in longitudinal data. In contrast, dynamic graph representation algorithms offer the ability to model evolving relationships over time and have been explored with some explainability efforts Wu et al. (2024); Zheng et al. (2024). However, to date, no prior work has effectively leveraged dynamic graph-based learning models to analyze longitudinal clinical features for understanding neural disorder diseases such as PD Zheng et al. (2024).

To uncover PD temporal disease stages, we constructed age-based graphs representing yearly clinical visits of patients based on their cerebrospinal fluid (CSF) peptide profiles. The goal of the proposed architecture is to generate a meaningful representation for each clinical visit, allowing these representations to be clustered and revealing distinct disease stages. We hypothesize that this is feasible if the learned embeddings emphasize local structure while also capturing each patient's disease trajectory over time. To achieve this, the model employs a single-layer GCN to extract spatial representations for each patient at a given age. These representations are then passed through a sequential model, such as a Gated Recurrent Unit (GRU), to learn generalized spatio-temporal patterns across time. The resulting temporal patterns are concatenated with age-specific spatial embeddings, and the combined representation is passed through fusion layers to produce node embeddings at each time step that capture both local structural dependencies and temporal progression.

The quality of the learned node representations by the multi-model was evaluated by comparing the clustering performance of embeddings against several baseline methods, including standard graph representation learning models (such as GCN, T-GCN, and GC-LSTM) and conventional feature representation techniques, such as dimensionality reduction methods and dense autoencoders.

The main contribution of this study demonstrates that the proposed multi-model graph learning approach outperforms existing feature representation methods in modeling longitudinal clinical data. This means that incorporating the general temporal progression of the nodes emphasized by their local spatial embeddings enabled the discovery of meaningful stages of disease progression. To the best of our knowledge, this is the first graph-based model to generate such comprehensive spatiotemporal representations for unsupervised learning in this context. Furthermore, this work presents the first application of dynamic graph learning models to uncover meaningful stages of neural disorder disease, specifically in PD.

2 Related work

108

109

110

111

112

113

114

115

116

117

118

119 120 121

122 123 124

125

126

127

128

129

130

131

132

133

134

135

136

137

138

139 140

141

142

143

144

145

146

147

148

149

150

151

152

153

154

155

156 157

158

159

160

161

Existing graph learning models like GCN Kipf & Welling (2017) are designed for static graphs and cannot capture evolving structures over time. However, temporal extensions in dynamic graph models such as T-GCN Zhao et al. (2020) and GC-LSTM Chen et al. (2022) integrate temporal sequences with learned structural patterns but remain limited to capturing only short-term historical temporal dependencies when modeling current graph nodes. Moreover, the Temporal Graph Network (TGN) Rossi et al. (2020) generates node embeddings through temporal message passing with memory modules. However, in its common edge-based implementation, TGN does not utilise node features in the embedding process, nor does it compute node embeddings at each graph snapshot or capture long-range temporal dynamics in all its existing implementations. Models like EvolveGCN Pareja et al. (2019) and DyGCN Gu et al. (2024) update weights or node states over time, yet fail to jointly model local spatial features and generalized node trajectories across snapshots. To the best of the authors' knowledge, none of the existing approaches are designed for unsupervised representation learning in age-based or longitudinal graphs, where each node evolves over time and must be embedded accordingly. The multi-model is designed to explicitly capture both spatial structure and generalized temporal patterns per node, enabling more meaningful representations for downstream unsupervised tasks like disease stages discovery. This contribution remains largely unexplored in the current literature.

From a healthcare perspective, GNNs are not new and have been primarily employed for representation learning, graph pooling, and entities generations (like molecules represented as graph nodes or edges), for applications dominated by structural and semantic relationships understanding among biological entities like molecular interactions, protein functions, tissue-specific gene regulation, and predict disease- phenotype-disease associations Li et al. (2022). For example, subgraph neural networks (SubGNNs), portions of a larger graph, have been applied to model diseases as phenotype subgraphs derived from the Human Phenotype Ontology (HPO) knowledge base, for disease classification tasks Li et al. (2022). Additionally, researchers in Abu Zohair et al. (2025) structured each patient's CSF longitudinal records into a single graph and applied GCNs to model disease trajectories. However, an LSTM autoencoder was shown to outperform this approach. This approach and the aforementioned applications were based on static graph structures and lacked the employment of temporal modeling in a dataset of longitudinal nature. Also, in critical care and infection control, models like MSTD-GNN and STM-GNN have used temporal attention and memory to model irregular ICU records and hospital-acquired infection dynamics, respectively, but remain largely prediction-focused and rely on learning historical temporal patterns Geissbuhler et al. (2025); Liu et al. (2025). Researchers also integrates dynamic attention into CTDGs by fusing global medical ontologies with patient-specific knowledge graphs, adjusting by the graph edge weights in real time to improve disease diagnosis Chen et al. (2025).

Despite these advancements, notable gaps persist. Subgraph-based disease models in prior work do not account for dynamic symptoms evolution. Very few studies explore dynamic graph modeling, but not in the context of learning representation for unsupervised tasks. Discrete and continuous-time dynamic graph models were employed. However, their efficiency in handling incomplete longitudinal records has not yet been addressed. Finally, the potential of dynamic graph models in modelling longitudinal records for understanding disease dynamics progression in rare or neurode-

generative diseases has yet to be explored. This research contribution directly addresses these limitations by introducing a fused GCN-GRU architecture that models the influence of local structural patterns in every graph snapshot node while learning every node's temporal progression dynamics, enabling the unsupervised grouping of distinct disease stages across various progression trajectories. Finally, this work pioneers the first dynamic graph approach for modeling Huntington's disease, offering insights into disease states that have never been captured in prior literature.

3 METHOD

3.1 Dataset

The dataset utilized in this study comprises longitudinal protein and peptide abundance profiles extracted from CSF samples collected from 248 patients, and was sourced from Kaggle Kirsch et al. (2023). In addition to CSF-derived peptide abundance data, the dataset also contains longitudinal clinical scores, specifically the UPDRS parts 1, 2, and 3, capturing mood and cognitive symptoms, abilities for daily living activities, and motor complications before and after medication, respectively Kirsch et al. (2023). Both datasets enable the temporal analysis of disease progression in PD, facilitating the development of computational models to infer disease states and patient trajectories, and understand some disease/patients characteristics in each discovered stage.

3.2 METHODS AND PROCEDURES

3.2.1 Conventional Feature Representation Methods

K-PCA and t-distributed stochastic neighbor (t-SNE), non-linear dimensionality reduction or latent representations of peptide types were selected as feature reduction techniques. This decision was made after preliminary analysis of data normality using the Shapiro-Wilk and Q-Q plots. In parallel, dense autoencoders were commonly outperformed for learning representations of patient records Sushil et al. (2018); Alkhayrat et al. (2020); Abu Zohair et al. (2025). In this project, a single-layer dense autoencoder was employed to learn the latent representation of patients' clinical visits. Following this, multiple graph representation learning models were explored. For example, a static GCN with a single convolution layer was applied to patient records structured in temporal clinical visit-based graphs, capturing only node structural patterns within a single graph. In addition, standard dynamic graph models, such as the T-GCN, extend the structural patterns (relationships among patient features within each clinical visit) learned by the GCN by incorporating connections to historical temporal patterns. In this work, a simplified implementation of T-GCN is presented, combining a single-layer GCN with a sequential model based on GRU. This design choice aims to avoid over-smoothing effects caused by aggregating higher-order adjacency neighbors, which can lead to homogenized node representations and the loss of node-specific local patterns. The following subsection presents the formal graph definitions and describes the architecture of the multi-model, which will be compared with the previously introduced approaches.

3.2.2 GRAPH STRUCTURE AND MULTI-MODEL DEFINITIONS

To utilize graph learning representation models, the tabular representation of the dataset was transitioned into a graph-based structure. Inspired primarily by Kazemi et al. (2020), an undirected graph was constructed at each clinical visit in the longitudinal dataset (based on the visit_month feature), as illustrated in Figure 1. This graph is annotated by $G=(\mathcal{V},\mathcal{E})$, where:

- \mathcal{V} be the set of vertices (nodes), representing patients, indexed by the patient_id feature.
- Peptide types and their abundances for each patient are stored as node features and represented in a matrix $\mathbf{X} \in \mathbb{R}^{n \times d}$, where n is the number of patients (nodes), and d is the number of clinical features associated with each node.
- \mathcal{E} be the set of edges added between nodes. An edge is added when the similarity (measured by Euclidean distance) between two patients' features is below a specified threshold. This graph structure is represented by an adjacency matrix $\mathbf{A} \in \mathbb{R}^{n \times n}$, defined as:

$$A_{ij} = \begin{cases} 1, & \text{if similarity between patients } i \text{ and } j \text{ features} \leq \text{threshold} \\ 0, & \text{otherwise} \end{cases}$$

> 223 224

The threshold corresponds to the 5th percentile of the pairwise Euclidean distance distribution between node features. It was aimed to retain only the strongest and most meaningful connections, while reducing noise from weaker or less informative similarities. The final threshold was determined by averaging the 5th percentile of Euclidean similarity distribution scores across all graphs.

225

226 227

232 233 234

235 236 237

239 240 241

242

243

244

238

250 251 252

253

249

258

265

266

267

268

269

G₁ G_t Time (Clinical Visits Months)

Figure 1: Temporal graph construction across clinical visits in the longitudinal dataset. Each node represents a patient's record at a specific clinical visit (based on the visit_month feature), with edges capturing the similarity between the features of two patients' nodes.

The implemented multi-model architecture, illustrated in Figure 2, employs GCN to generate spatial node embeddings (e_S) at each graph snapshot, which are then fed into a GRU model to capture general spatial dependencies (within and across patients' features) and temporal dynamics (across visits), including current, historical, and future patterns (e_t) . Finally, the learned spatio-temporal pattern for each node is concatenated with its spatial embedding at every clinical visit and passed through fusion layers to generate node representations (e_{t+S}) , which are then used in an unsupervised clustering algorithm to identify disease states.

By definition, the multi-model creates latent node embeddings for nodes at each age using a single layer of GCN encoder (GCNConv layer- graph convolution layer provided by PyTorch Geometric) from the standard implementation of static GCN Kipf & Welling (2017), Jiang et al. (2019). These embeddings are created by simply convolving over a node's direct neighbors, as defined by Equation 1.

$$H_t = \sigma(\hat{A}_t X_t W),\tag{1}$$

where: H_t are the node embeddings of graph at clinical visit t, A_t is the normalized adjacency matrix at clinical visit t, W_t is the learnable weight matrix at clinical visit t, and σ is the activation function (ReLU) that combines the graph structure and node features X to compute the updated node embeddings.

After that, the spatial embeddings (e^s) created for each node at each time-step (age) were fed to a single GRU layer to create a single spatio-temporal embedding for the dynamics of each patient's features. It is worth noting that this implementation of T-GCN is slightly modified from its standard implementation by Zhao et al. (2020), with a reduced number of GCN layers used to compute the spatial nodes' embeddings. Additionally, the node embedding from each GRU hidden state for each node at each age (which accounts for both current and historical temporal patterns) was also extracted to assess its representativeness in discovering the disease state compared to the proposed one. By definitions, for each patient (node n), the spatial embeddings over time form this sequence $H_{n0}, H_{n1}, \dots, H_{nt}$, where t denotes clinical visit time. The spatial embeddings for each node are then fed into a GRU and produce a sequence of hidden states $Z_{n0}, Z_{n1}, \dots, Z_{nt}$ where Z_{nt} is the GRU's hidden state for node n at clinical visit t. This is defined in Equation 2;

$$Z_{nt} = \text{GRU}(H_{n0}, H_{n1}, H_{n2}, \dots, H_{nt})$$
 (2)

The spatial-general temporal embedding, annotated by e^t in Figure 2, created for each patient (n) at last clinical visit (t) defined as $Z_n = Z_{1t}, Z_{2t}, Z_{3t}, \ldots, Z_{nt}$. This will be used to create the final node embedding, e^{s+t} in Figure 2, for each node n at each time step (t) by fusing it with the spatial nodes' embeddings created at each age (H_{nt}) by Equation 3.

 $F_{nt} = \text{Fusion}([H_{nt} \parallel Z_{nt}]),\tag{3}$

where: \parallel denotes concatenation, and $F_{nt} \in \mathbb{R}^{N \times d}$ is the proposed model embedding for all nodes at every age t. Fusion corresponds to the fusion layers (illustrated in Figure 1), which apply a fully connected layer to the concatenated embeddings H_{nt} and Z_{nt} , projecting them into a fixed fusion dimension (fusion_dim). A ReLU activation is applied to the output to introduce nonlinearity and help capture complex relationships. Then, it is finally passed through a normalization layer (LayerNorm) to stabilize training and improve convergence. The used Fusion layers were frequently employed when combining embeddings of features from multiple models or data modalities resources in the literature Liu et al. (2020), Li et al. (2017). The selection of these layers was done progressively, while assessing model training loss simultaneously, resulting with the final configuration chosen based on achieving the lowest model loss. The explained model components were

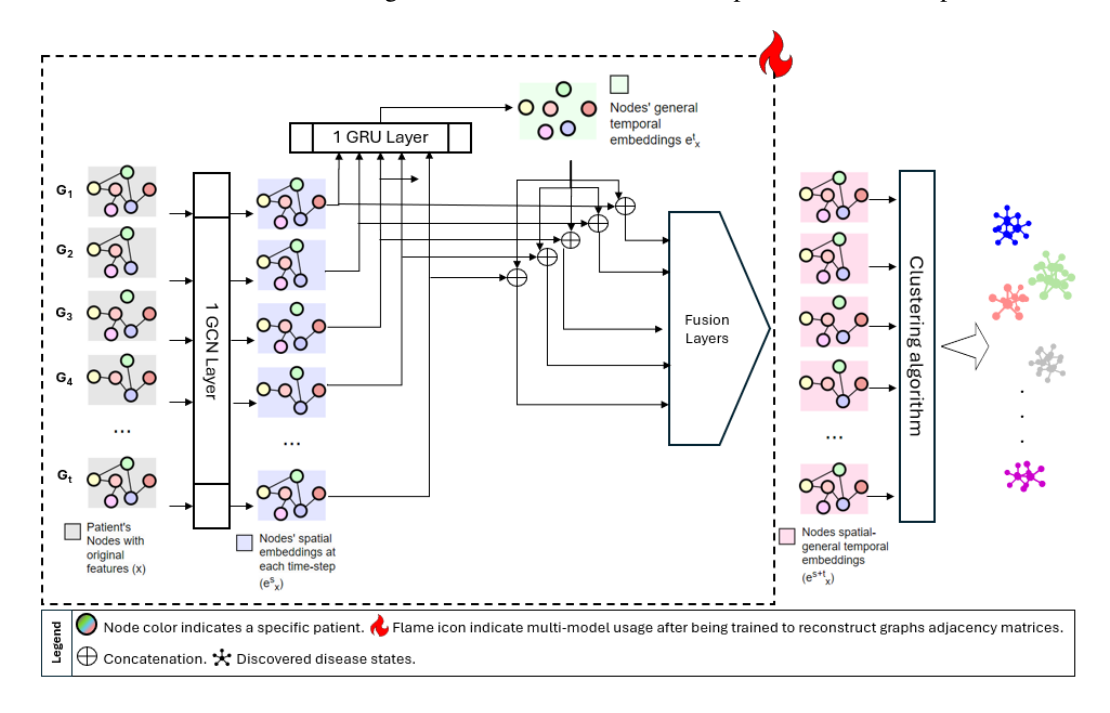


Figure 2: Overview of the Proposed Dynamic Graph Model Architecture. G_{1-t} represents the graphs constructed at each unique age in the longitudinal clinical visits' dataset. Each node color represents a unique patient who attended a clinical visit at the corresponding age. Missing nodes indicate time points where patients did not attend a clinical visit. The letter x to denote original features, e for features' embeddings, where superscript S refers to the spatial embeddings and superscript t denotes the temporal embeddings generated for each patient

trained (surrounded by dotted rectangles with flame icon in Figure 2) to reconstruct the graph structure using a binary cross-entropy loss over the predicted adjacency matrices Kipf & Welling (2016). Once trained, node embeddings were computed by the model for each node at each age graph; illustrated by the graphs with a pink background in Figure 1. These embeddings, as well as the T-GCN hidden state embeddings (Z_{nt}), which capture both current and historical temporal patterns in addition to structural information, were passed to the clustering phase. Clustering performance will determine the representativeness of multi-model embeddings compared to conventional embedding learning approaches or direct feature clustering in discovering distinct groups of patterns that correspond to different but meaningful PD disease states. Models' hyperparameters and latent dimensions of the learned representations in all employed models were selected through a grid search, with the optimal dimension chosen based on the one that produced the lowest training loss after 250 epochs, after which the loss curve stabilized.

3.2.3 EXPERIMENTAL DESIGN

The analysis started with visualizations and descriptive statistics to understand feature characteristics, including general temporal trends in peptide counts, UPDRS score progression patterns, and available patients clinical records per visit. Patients with richer longitudinal data were filtered and selected to better capture peptide trends over disease progression. Dataset pre-processing techniques, including zero imputation of empty peptide abundance, label encoding, and features' normalization using RobustScaler (known for better outliers handling Izonin et al. (2022)), ensured the data was normalized and suitable for both classical and deep learning models.

To further examine and validate the underlying structure and distribution of the data before selecting appropriate dimensionality reduction techniques and suitable statistical analysis methods, a series of statistical tests was conducted. Shapiro–Wilk and visualization of Q-Q plots were used to assess the data normality. Therefore, kernel principal component analysis (K-PCA) and t-distributed stochastic neighbor (t-SNE), non-linear dimensionality reduction or latent representations of peptide types, were selected as feature reduction techniques. Additionally, the normality test results in choosing the Kruskal–Wallis test to evaluate the significant differences in the distribution of UPDRS 1, 2, and 3 across the discovered disease states. Dunn's test was then applied to identify which cluster exactly differed significantly from each other in terms of UPDRS score. The formulated null hypothesis states that there is no significant differentiation among the discovered disease stages and UPDRS scores distribution, and a p-value threshold of 0.05 was set to reject it. Collectively, these statistical evaluations provided a robust foundation for selecting both classical feature reduction methods and assessing the significance of the discovered temporal pattern groups.

KMeans++ clustering algorithm was used, known to provide statistical assurance on the quality of the clustering Li et al. (2023). The quality of the clusters decides the optimal representation model performance, and is evaluated using 1) clustering metrics: Silhouette Score, Davies-Bouldin Index, and Calinski-Harabasz Score, and 2) the aforementioned significant test in the formulated hypothesis. The best number of clusters was selected based on the grid search k value that results in the best Silhouette score.

4 RESULTS AND DISCUSSIONS

A total of 24 patients with up to 6 years of clinical visits and 968 unique peptide types were selected for the analysis. Initially, the original peptide values were directly clustered. Then, dimensionality reduction and embedding methods were employed to better capture the underlying structure of peptides progression patterns. Specifically, t-SNE, K-PCA, and dense autoencoders, with 2-dimensional embeddings that consistently achieved the highest clustering scores across evaluation metrics. In addition, graph- and sequence-based neural models were applied to capture more complex patterns within a single patient's peptides, across patients in a single visit, and the progression of peptide expression over time. These included GCN, T-GCN, GS-LSTM, and the new Multi-Model architecture. Across all graph representation learning models, the optimal hyperparameters were commonly found to be a GCN embedding dimension of 8 and a GRU hidden dimension of 4, which yielded low training loss and strong clustering performance.

According to Figure 3, both the Multi-Model and GCN architectures achieved the highest clustering scores, but the Multi-Model consistently converged to 4 clusters, indicating a stable temporal disease state representation. Instead, the GCN lack stability in clustering performance across various seeds. The seed was initially set with a fixed random value to ensure that all sources of randomness, especially those caused by model weight initialization, behave deterministically across processing. This guarantees that the graph model's training, evaluation, and inference are fully reproducible, which was critical for fair comparisons.

However, model stability was a critical factor in evaluating the reliability of learned representations for disease stage discovery. The variability in clustering results was assessed across 10 different seeds for both the GCN and Multi-Model architectures. As shown in Table 1, the variability analysis based on standard deviation indicates that, although the clustering performance remained relatively stable, the GCN model's estimated number of clusters (K) fluctuated between 3 and 9. This was accompanied by substantial variation in the corresponding Calinski-Harabasz (CH) score. In con-

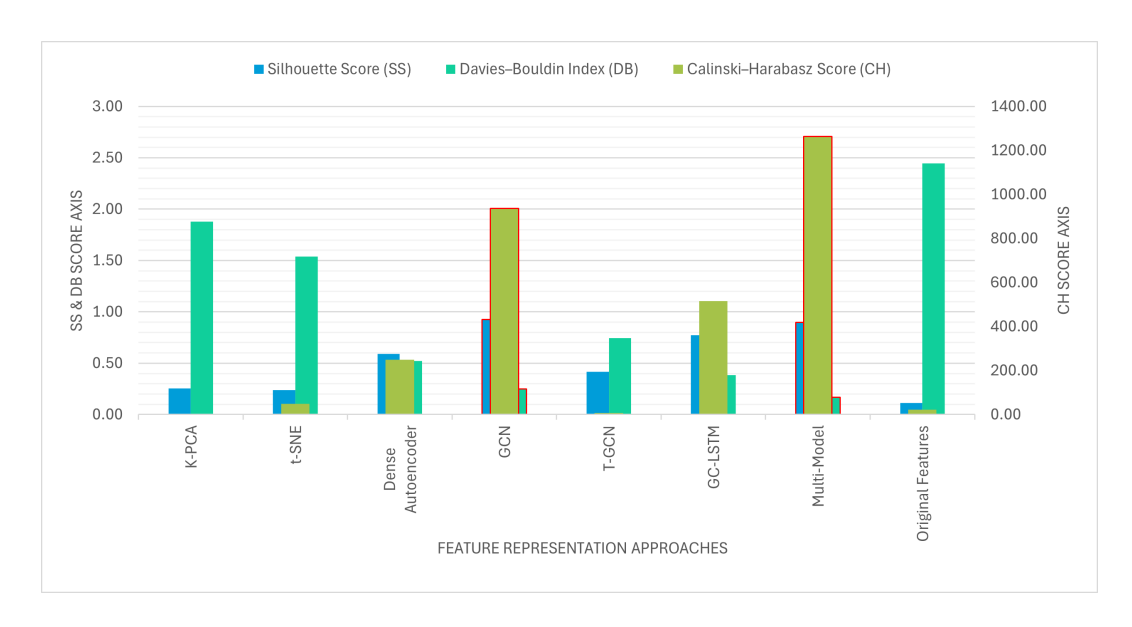


Figure 3: Clustering performance metrics results of peptides structural and/or temporal representations created by multiple feature representation Methods, including the new graph Multi-Model.

Table 1: Standard deviation of clustering metrics across 10 different seeds for GCN and Multi-Model. Lower values indicate higher stability.

Metric/Clusters	GCN (SD)	Multi-Model (SD)
G.11	0.02	0.04
Silhouette Score (SS)	0.02	0.04
Davies-Bouldin (DB)	0.08	0.14
Calinski-Harabasz (CH)	57,110.58	323.84
Number of Clusters (K)	1.79	0.46

trast, the Multi-Model architecture demonstrated markedly greater stability—consistently producing 4 clusters and yielding relatively stable clustering scores across all seeds (see Table A1).

To explain the disease stages from clinical perspectives, patients peptides dataset, including the discovered cluster, was merged with the UPDRS scores dataset - both originating from the same data source - using patient_id and visit_month as keys. Then, clusters formed by the Multi-Model, which demonstrated strong internal validity as indicated by its Davies-Bouldin (0.169) and Calinski-Harabasz indexes (1264.24), were analyzed. To facilitate this and unlock the severity of disease stages based on these scores, a box plot of the distribution of UPDRS scores across the discovered clusters was generated (see Figure 4).

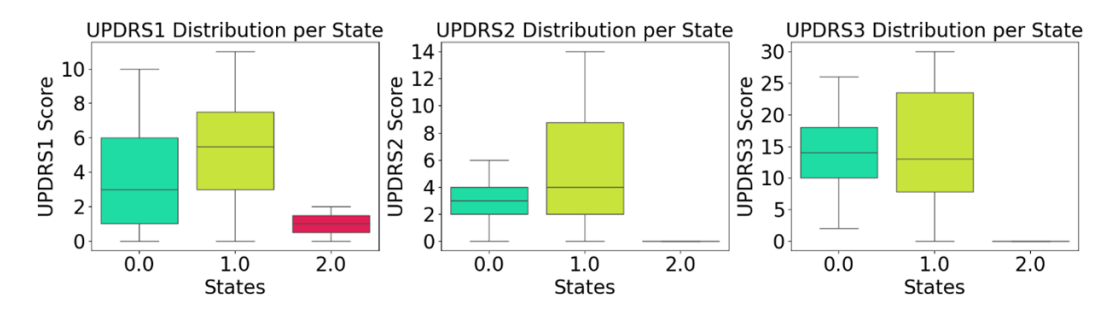


Figure 4: Box plot for the distribution of UPDRS 1, 2, & 3 scores across the discovered clusters.

It is important to note that one cluster appears missing in this figure. This was due to the exclusion of patients without corresponding UPDRS scores during the dataset merging process. As a result, (cluster 4) are not represented in the final UPDRS-based analysis. Kruskal-Wallis test revealed statistically significant differences ($p \le 0.05$) in both UPDRS Part 2 (motor experiences of daily living) and Part 3 (motor examination) scores across the plotted clusters. These differences are illustrated in Figure 4. A post-hoc Dunn's test was conducted to determine pairwise differences between clusters. This analysis, with 5, reveals that UPDRS Part 2 scores showed a significant difference between clusters 1 and 2 (p = 0.0306), with cluster 1 represent more sever UPDRS 2 symptoms compared to 2. For UPDRS Part 3, the differences were more pronounced, with cluster 2 exhibiting distinctly lower motor scores compared to clusters 0 and 1. In contrast, UPDRS Part 1 (non-motor experiences) was more evenly distributed across three clusters, but did not reach statistical significance (p = 0.11). This indicates that while the clustering effectively defines disease stages based on motor

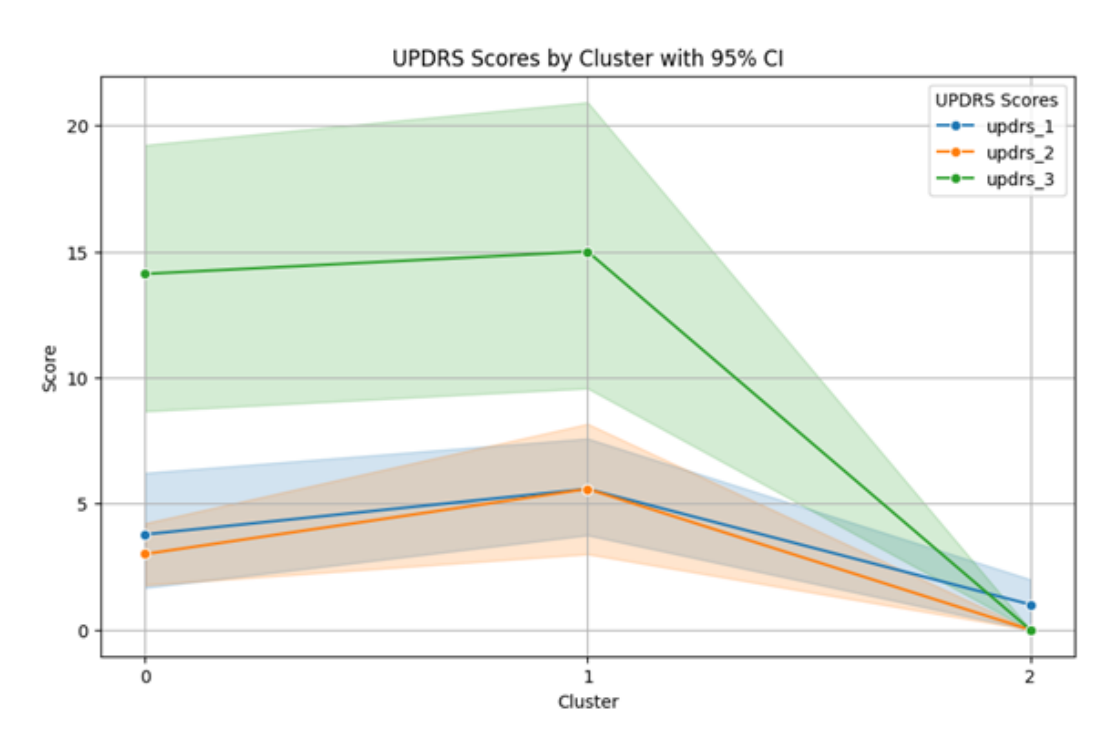


Figure 5: Mean UPDRS scores (Parts 1, 2, and 3) across discovered clusters, visualized with connected lines. Standard deviations are represented by shaded areas. This plot illustrates the variability in scores between the discovered clusters.

symptoms, it may be less sensitive to non-motor symptoms. These findings suggest that Cluster 1 reflects significant severe impairment in motor function and daily living activities for PD patients, while Cluster 2 groups those with mild symptoms of the disease. Despite the limited size of the dataset, the identified clusters capture clinically meaningful variation in motor symptom severity.

Future work will aim to reproduce these assessments in larger populations and further optimize the multi-model architecture by incorporating sequential models such as LSTM. Additionally, comparisons between multiple linear perceptrons (MLPs) in place of GCN will be explored. This enables us to evaluate the actual contribution of the graph structure (adjacency matrix) to the learning process. Since MLPs do not use connectivity information, they serve as a strong baseline to evaluate whether leveraging structural relationships in GCN causes a performance gain or if it is largely due to node features. Additionally, experimenting with alternative distance and similarity measures for edge construction, such as cosine similarity, will be explored. This proposed multi-model approach has demonstrated efficiency as a proof of concept, and future research will investigate its applicability to other neurodegenerative diseases as well as non-healthcare longitudinal datasets.

ETHICS STATEMENT

This research utilized publicly available dataset and does not include human subjects, sensitive data, or applications with foreseeable potential for harm. To the best of the authors' knowledge, our research has no ethical concerns related to fairness, privacy, security, or legal compliance.

This manuscript was written using Overleaf, and the coding and analysis were conducted in Google Colab. During that time, various AI solutions were auto-suggested for text writing, code generation, and, not to mention, the facility for code debugging and error resolution. However, all generated content was critically reviewed, modified where necessary, and validated to ensure that it fulfilled its intended purpose and maintained scientific rigor. While using these tools to improve productivity and resolve technical issues, the author ensured that the main work, including critical reasoning, ideation, and interpretative decisions, remained fully under the author's control, thereby preserving the originality and integrity of this work.

REPRODUCIBILITY STATEMENT

The dataset used in this study is publicly available and can be downloaded directly from https://www.kaggle.com/c/amp-parkinsons-disease-progression-prediction. All the code used for data preprocessing, analysis, and modeling is openly accessible at https://github.com/LubnaM/Graph_Multi-Model, ensuring full transparency and reproducibility of the results presented in this paper.

REFERENCES

- Lubna Mahmoud Abu Zohair, Hind Zantout, Marta Vallejo, and Md Azher Uddin. Unsupervised machine learning using cerebrospinal fluid proteomics for understanding parkinson's disease progression. *Proceedings of the AAAI Symposium Series*, 6(1):72–74, Aug. 2025. doi: 10.1609/aaaiss.v6i1.36033. URL https://ojs.aaai.org/index.php/AAAI-SS/article/view/36033.
- Maha Alkhayrat, Mohamad Aljnidi, and Kadan Aljoumaa. A comparative dimensionality reduction study in telecom customer segmentation using deep learning and pca. *Journal of Big Data*, 7(1): 9, Feb 2020. ISSN 2196-1115. doi: 10.1186/s40537-020-0286-0. URL https://doi.org/10.1186/s40537-020-0286-0.
- R. Balestrino and A.H.V. Schapira. Parkinson disease. *European Journal of Neurology*, 27(1):27–42, 2020. doi: https://doi.org/10.1111/ene.14108. URL https://onlinelibrary.wiley.com/doi/abs/10.1111/ene.14108.
- Deng Chen, Weiwei Zhang, and Zuohua Ding. Embedding dynamic graph attention mechanism into clinical knowledge graph for enhanced diagnostic accuracy. *Expert Systems with Applications*, 267:126215, 2025. ISSN 0957-4174. doi: https://doi.org/10.1016/j.eswa. 2024.126215. URL https://www.sciencedirect.com/science/article/pii/S0957417424030823.
- Jinyin Chen, Xueke Wang, and Xuanheng Xu. Gc-lstm: graph convolution embedded lstm for dynamic network link prediction. *Applied Intelligence*, 52(7):7513–7528, May 2022. ISSN 0924-669X. doi: 10.1007/s10489-021-02518-9. URL https://doi.org/10.1007/s10489-021-02518-9.
- Jasper de Jong, Md Asif Emon, Pei Wu, Roshan Karki, Mohit Sood, Philippe Godard, Akram Ahmad, Henri Vrooman, Martin Hofmann-Apitius, and Holger Fröhlich. Deep learning for clustering of multivariate clinical patient trajectories with missing values. *GigaScience*, 8(11):giz134, 2019. doi: 10.1093/gigascience/giz134.
- Jiahao Gan, Zhijian Peng, Xiaolei Zhu, Rui Hu, Jun Ma, and Guorong Wu. Brain functional connectivity analysis based on multi-graph fusion. *Medical Image Analysis*, 71:102057, Jul 2021. doi: 10.1016/j.media.2021.102057. Epub 2021 Apr 9.

Damien Geissbuhler, Alban Bornet, Catarina Marques, André Anjos, Sónia Pereira, and Douglas Teodoro. Stm-gnn: Space-time-and-memory graph neural networks for predicting multidrug resistance risks in dynamic patient networks. *medRxiv*, 2025. doi: 10.1101/2025. 05.27.25327491. URL https://www.medrxiv.org/content/early/2025/05/28/2025.05.27.25327491.

- Yonghao Gu, Xiaoqing Zhang, Hao Xu, and Tiejun Wu. Dygcn: Dynamic graph convolution network-based anomaly network traffic detection. In 2024 IEEE 23rd International Conference on Trust, Security and Privacy in Computing and Communications (TrustCom), pp. 1838–1843, 2024. doi: 10.1109/TrustCom63139.2024.00253.
- Ivan Izonin, Bohdan Ilchyshyn, Roman Tkachenko, Michal Greguš, Natalya Shakhovska, and Christine Strauss. Towards data normalization task for the efficient mining of medical data. In 2022 12th International Conference on Advanced Computer Information Technologies (ACIT), pp. 480–484, 2022. doi: 10.1109/ACIT54803.2022.9913112.
- Bo Jiang, Ziyan Zhang, Doudou Lin, Jin Tang, and Bin Luo. Semi-supervised learning with graph learning-convolutional networks. In *2019 IEEE/CVF Conference on Computer Vision and Pattern Recognition (CVPR)*, pp. 11305–11312, 2019. doi: 10.1109/CVPR.2019.01157.
- Seyed Mehran Kazemi, Rishab Goel, Kshitij Jain, Ivan Kobyzev, Akshay Sethi, Peter Forsyth, and Pascal Poupart. Representation learning for dynamic graphs: A survey, 2020. URL https://arxiv.org/abs/1905.11485.
- Thomas N. Kipf and Max Welling. Variational graph auto-encoders. arXiv, 2016.
- Thomas N. Kipf and Max Welling. Semi-supervised classification with graph convolutional networks, 2017. URL https://arxiv.org/abs/1609.02907.
- L. Kirsch, S. Dane, S. Adam, and V. Dardov. AMP®-Parkinson's Disease Progression Prediction. https://kaggle.com/competitions/amp-parkinsons-disease-progression-prediction, 2023. Kaggle competition.
- Angeliki Kouli, Katherine M. Torsney, and Wen-Lang Kuan. Parkinson's disease: Etiology, neuropathology, and pathogenesis. In Thomas B. Stoker et al. (eds.), *Parkinson's Disease: Pathogenesis and Clinical Aspects*. Codon Publications, 2018. doi: 10.15586/codonpublications.parkinsonsdisease.2018.chl. URL https://doi.org/10.15586/codonpublications.parkinsonsdisease.2018.chl.
- Fan Li, Danni Cheng, and Manhua Liu. Alzheimer's disease classification based on combination of multi-model convolutional networks. In *2017 IEEE International Conference on Imaging Systems and Techniques (IST)*, pp. 1–5. IEEE, 10 2017. ISBN 978-1-5386-1620-8. doi: 10.1109/IST.2017. 8261566.
- Hao Li, Haolin Zhang, Hans Johnson, Jody D. Long, Jane S. Paulsen, and Ipek Oguz. Longitudinal subcortical segmentation with deep learning. In *Proceedings of SPIE–the International Society for Optical Engineering*, volume 11596, pp. 115960D, 2021. doi: 10.1117/12.2582340.
- Mi Li, Eibe Frank, and Bernhard Pfahringer. Large scale k-means clustering using gpus. *Data Mining and Knowledge Discovery*, 37:67–109, 1 2023. ISSN 1384-5810. doi: 10.1007/s10618-022-00869-6.
- Michelle M. Li, Kexin Huang, and Marinka Zitnik. Graph representation learning in biomedicine and healthcare. *Nature Biomedical Engineering*, 6(12):1353–1369, 2022. doi: 10.1038/s41551-022-00942-x.
- Guanlin Liu, Xiaomei Yu, Zihao Liu, Xue Li, Xingxu Fan, and Xiangwei Zheng. Dnmdr: Dynamic networks and multi-view drug representations for safe medication recommendation, 2025. URL https://arxiv.org/abs/2501.08572.

- Manhua Liu, Fan Li, Hao Yan, Kundong Wang, Yixin Ma, Li Shen, and Mingqing Xu. A multi-model deep convolutional neural network for automatic hippocampus segmentation and classification in alzheimer's disease. *NeuroImage*, 208:116459, 3 2020. ISSN 10538119. doi: 10.1016/j.neuroimage.2019.116459.
 - Yuan Luo, Lijun Qiao, Mengyao Li, Xiaoyu Wen, Wei Zhang, and Xia Li. Global, regional, national epidemiology and trends of parkinson's disease from 1990 to 2021: findings from the global burden of disease study 2021. *Frontiers in Aging Neuroscience*, 16:1498756, Jan 2025. ISSN 1663-4365. doi: 10.3389/fnagi.2024.1498756.
- Aldo Pareja, Giacomo Domeniconi, Jie Chen, Tengfei Ma, Toyotaro Suzumura, Hiroki Kanezashi, Tim Kaler, Tao B. Schardl, and Charles E. Leiserson. Evolvegen: Evolving graph convolutional networks for dynamic graphs, 2019. URL https://arxiv.org/abs/1902.10191.
- Emanuele Rossi, Benjamin Paul Chamberlain, Fabrizio Frasca, Davide Eynard, Federico Monti, and Michael M. Bronstein. Temporal graph networks for deep learning on dynamic graphs. *ArXiv*, abs/2006.10637, 2020. URL https://api.semanticscholar.org/CorpusID:219792342.
- Dong-Woo Ryu, Kyungdo Han, and Ah-Hyun Cho. Mortality and causes of death in patients with parkinson's disease: a nationwide population-based cohort study. *Frontiers in Neurology*, 14: 1236296, 2023. doi: 10.3389/fneur.2023.1236296.
- Junyuan Shang, Cao Xiao, Tengfei Ma, Hongyan Li, and Jimeng Sun. Gamenet: Graph augmented memory networks for recommending medication combination. *Proceedings of the AAAI Conference on Artificial Intelligence*, 33(01):1126–1133, Jul. 2019. doi: 10.1609/aaai.v33i01.33011126. URL https://ojs.aaai.org/index.php/AAAI/article/view/3905.
- Dong Su, Yujia Cui, Cheng He, et al. Projections for prevalence of parkinson's disease and its driving factors in 195 countries and territories to 2050: modelling study of global burden of disease study 2021. *BMJ*, 388:e080952, Mar 2025. doi: 10.1136/bmj-2024-080952. Published 2025 Mar 5.
- Madhumita Sushil, Simon Suster, Kim Luyckx, and Walter Daelemans. Patient representation learning and interpretable evaluation using clinical notes. *Journal of Biomedical Informatics*, 84: 103–113, 2018. ISSN 1532-0464. doi: https://doi.org/10.1016/j.jbi.2018.06.016. URL https://www.sciencedirect.com/science/article/pii/S1532046418301266.
- Guanlin Wu, Ke Yu, Hao Zhou, Xiaofei Wu, and Sixi Su. Time-series anomaly detection based on dynamic temporal graph convolutional network for epilepsy diagnosis. *Bioengineering*, 11(1), 2024. ISSN 2306-5354. doi: 10.3390/bioengineering11010053. URL https://www.mdpi.com/2306-5354/11/1/53.
- Ling Zhao, Yujiao Song, Chao Zhang, Yu Liu, Pu Wang, Tao Lin, Min Deng, and Haifeng Li. T-gcn: A temporal graph convolutional network for traffic prediction. *IEEE Transactions on Intelligent Transportation Systems*, 21(9):3848–3858, 2020. doi: 10.1109/TITS.2019.2935152.
- Yanping Zheng, Lu Yi, and Zhewei Wei. A survey of dynamic graph neural networks. *Frontiers of Computer Science*, 19(6):196323, 2024. ISSN 2095-2236. doi: 10.1007/s11704-024-3853-2. URL https://doi.org/10.1007/s11704-024-3853-2.
- Çağatay Berke Erdaş, Emre Sümer, and Seda Kibaroğlu. Neurodegenerative disease detection and severity prediction using deep learning approaches. *Biomedical Signal Processing and Control*, 70:103069, 2021. ISSN 1746-8094. doi: https://doi.org/10.1016/j.bspc. 2021.103069. URL https://www.sciencedirect.com/science/article/pii/S1746809421006662.

A APPENDIX

Table A1: Clustering scores across 10 different seeds for GCN and Multi-Model. SS: Silhouette Score, DB: Davies-Bouldin, CH: Calinski-Harabasz, K: Number of clusters.

		GCN		
Seed	SS	DB	СН	K
0	0.9508	0.2548	2,458.85	7
12	0.9508	0.2548	8,622.10	6
22	0.9708	0.1234	13,888.18	5
32	0.9843	0.0278	189,078.22	4
42	0.9682	0.2481	6,095.28	6
52	0.9491	0.2777	4,819.29	8
62	0.9576	0.3202	1,422.66	4
72	0.9282	0.2829	915.69	5
82	0.9877	0.0790	4,690.02	3
92	0.9264	0.3313	1,716.94	9

	Multi-Model						
Seed	SS	DB	СН	K			
0	0.8491	0.2606	467.83	3			
12	0.8494	0.3491	695.68	4			
22	0.7854	0.6502	252.38	3			
32	0.8465	0.2366	322.02	4			
42	0.8958	0.1694	1,264.24	4			
52	0.9056	0.3463	645.35	4			
62	0.7975	0.4103	406.15	4			
72	0.9040	0.3430	843.84	4			
82	0.8635	0.4895	307.84	4			
92	0.7684	0.6719	205.83	4			